

Pinning Transition of Bose-Einstein Condensates in Optical Ring Resonators

S. C. Schuster,^{*} P. Wolf, D. Schmidt, S. Slama, and C. Zimmermann[†]
*Physikalisches Institut, Eberhard-Karls-Universität Tübingen,
 Auf der Morgenstelle 14, D-72076 Tübingen, Germany.*

We experimentally investigate the dynamic instability of Bose-Einstein condensates in an optical ring resonator that is asymmetrically pumped in both directions. We find that, beyond a critical resonator-pump detuning, the system becomes stable regardless of the pump strength. Phase diagrams and quenching curves are presented and described by numerical simulations. We discuss a physical explanation based on a geometric interpretation of the underlying nonlinear equations of motion.

For several years, atomic quantum gases in optical resonators have been successfully used to study basic many-body physics with long-range interaction. Quantum phase transitions, supersolid phases and the realization of synthetic gauge fields are some of the current topics of this field [1–6]. While, so far, most experiments have been performed with standing wave resonators, the specific properties of ring resonators are now coming to the fore again [7, 8]. In contrast to standing wave resonators, in an ideal ring resonator, the position of the nodes and antinodes of an optical standing wave is not determined by end mirrors. However, in the presence of atoms and with sufficiently strong pumping power, this continuous symmetry can be broken spontaneously. The associated instability was already predicted in 1998 and interpreted as an analogy to the free-electron laser [9]. The effect was also observed experimentally more than a decade ago [10, 11], but, only recently, was it possible to record a complete stability diagram [12, 13]. These latest experiments also confirmed a model that interprets the instability as a generalization of the Dicke phase transition [1, 14, 15]. Experiments with ring resonators pumped simultaneously in both directions have not yet been conducted. This Letter makes a first contribution in this direction.

In a longitudinally pumped ring cavity, as shown in Fig. 1, the prominent effect is an exponential instability that is observed above a critical pump power: If some light is present in the probe mode, the interference pattern between the pump and the probe light generates a periodic optical potential, which structures the initially flat atomic density distribution. The resulting density grating efficiently diffracts pump light into the probe mode. This, in turn, deepens the optical lattice, and also, as a consequence, the atomic density grating increases its contrast and so on. During the process, momentum is constantly transferred from the pump mode to the probe mode and the atoms accelerate into the direction of the pump light (to the right in Fig. 1). Parallel to the atomic motion, the Doppler effect shifts the frequency of the diffracted probe light to lower frequencies. In this work, we extend the scenario and inject some light into the probe mode that has the same frequency as the

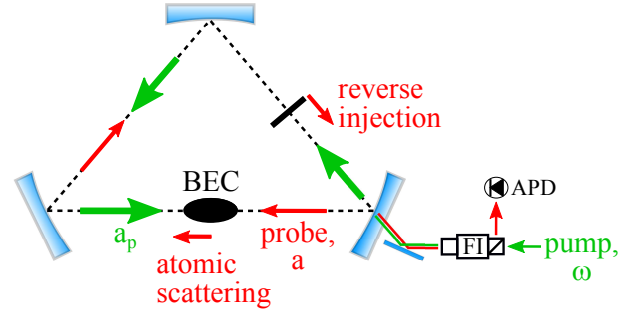


FIG. 1: Experimental setup of a BEC placed in a high-finesse TEM₀₀ mode of a ring resonator. Light from the pump mode (green, *s* pol.) is scattered into the probe mode (red) by the atoms and by coherent scattering at the mirror (here, represented by an effective reflecting element labeled “reverse injection”). The power in the probe mode is monitored by recording the probe light that leaves the cavity through the input coupling mirror. It is separated from the pump light with a Faraday isolator and detected with an avalanche photodiode (APD).

pump light. Together with the pump light, it forms a stationary optical lattice that might force the atoms to rest and suppresses the instability. Surprisingly, we find that there is a critical detuning of the cavity relative to the pump light. Above this detuning, the system is always stable. Below the critical detuning, the system is still unstable for large enough pump power. In this Letter we experimentally investigate this yet unknown “pinning transition” and compare our observations with numerical simulations of the nonlinear equations of motion. Furthermore, we present a geometric interpretation of the equations, which reveals the underlying physical mechanism.

The experimental setup in Fig. 1 is similar as described in [12]; however, now, use a much larger resonator with a round trip length of 39 cm, a beam waist at the position of the condensate of $w_0 = 170 \mu\text{m}$ and a mode volume of $V = 18.2 \text{ mm}^3$. For *s*-polarized light, the decay rate for the electric field amplitude in the resonator amounts to $\kappa = 2\pi \cdot 5 \text{ kHz}$ which is about three times smaller than the recoil shift $\omega_r = 2\hbar k^2/m = 2\pi \times 14.5 \text{ kHz}$ due to momentum absorption of an initially nonmoving atom that scat-

ters a photon from a pump beam into the probe beam. Here, k and m are the wave vector of the pump light and the mass of the atom. For p -polarized light, we observe a three times larger decay rate. The s -polarized forward propagating TEM₀₀ mode (“pump mode”) is longitudinally pumped from one side with up to 6 mW from an amplified diode laser system at a frequency ω detuned by $\Delta_a = \omega - \omega_0 = -60$ GHz relative to the atomic transition frequency ω_0 ($D1$ Line: $5s_{1/2}, F = 2$ to $5p_{1/2}, F = 2$). Part of the laser output is used to electronically stabilize the laser to the reverse propagating p -polarized TEM₁₀ mode [16] with a precision of about $2\pi \times 200$ Hz. Frequency and amplitude of the pump light is controlled by an acousto-optical modulator. The pump frequency ω can be tuned relative to the resonance frequency ω_c of the TEM₀₀ mode over a range of $\Delta_c = \omega_c - \omega = \pm 10\omega_r$. The power in the TEM₀₀ pump mode and in the counter-propagating TEM₀₀-mode (probe mode) is monitored by recording the light leaking out of the resonator mirrors with sensitive avalanche diodes.

The pinning potential required to suppress the instability beyond the critical detuning is very small such that we don’t have to inject the probe mode externally, but rather exploit coherent scattering of pump light into the probe mode due to inhomogeneities in the mirror coatings. The scattered light from the three mirrors interferes according to their relative positions and to the wavelength of the light [17]. The total mirror scattering can be varied up to a factor of 3 by controlling the position of one of the mirrors with a piezoelement. In the experiment, the total mirror scattering rate $\kappa_s = \kappa\sqrt{\varepsilon}$ is determined for each cycle by recording the resonant power ratio ε of the pump and the probe mode right before the atoms are loaded into the cavity. The magnetically trapped Bose-Einstein condensate of ⁸⁷Rb atoms is placed at the intensity minimum in the center of the TEM₁₀ mode where the atoms are least affected by the locking light. During preparation of the condensate, the laser beams are switched off and held at one fixed frequency for about 20 s. Once the condensate is in place, the locking is reactivated within 300 ms and the pump light is then ramped up to a final value within 50 μ s, slow enough to avoid ringing of the high finesse resonator. After a holding time of 1.5 ms, the atoms are released from the trap and the population of the momentum states are derived from absorption images after 35 ms of ballistic expansion. Data are taken from 20 000 experimental cycles for various cavity pump detunings Δ_c and photon numbers $|a_p|^2$ in the pump mode. The data are post selected according to the value of the ratio $R := \kappa_s / (2U_0N)$ for the specific cycle. The denominator contains the total number of atoms N and the single photon light shift $U_0 = g_{\text{eff}}^2 / \Delta_a$ with the coupling constant $g_{\text{eff}} = \frac{\omega d^2}{6\hbar\varepsilon_0 V} = 2\pi \times 19$ kHz, the dipole moment of the atomic transition d , and the permittivity of free space ε_0 . The ratio R turns out to be the relevant

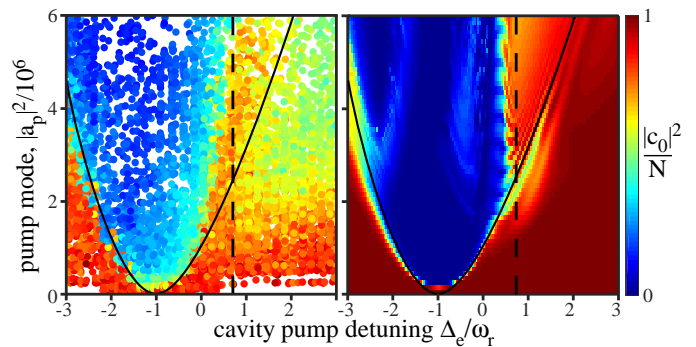


FIG. 2: Phase diagram. Population of the zero momentum state after 1.5ms of interaction with the light in the resonator for various photon numbers in the pump mode and cavity pump detuning. For negative detuning, the experimental observations (left subplot) are well described by the phase boundary derived from a numerical simulation that does not include the pinning potential (solid line). The simulation shown in the right subplot includes the pinning potential. The dashed line indicates the critical detuning within the limit of strong pumping according to Eq. (5).

parameter to specify the strength of the pinning potential (see theory part below). Figure 2 shows the observed population $|c_0|^2$ of the zero momentum state in the case of large mirror scattering ($R = 0.15$), a mean atom number in the BEC of $N = 1.8 \times 10^5$ and a atomic density of $5.7 \times 10^{12} \text{ cm}^{-3}$. The detuning $\Delta_e = \Delta_c + U_0N$ plotted along the horizontal axis is corrected for the index of refraction due to the atoms. The blue area, where the system is unstable and almost all atoms are excited into higher momentum states, is clearly separated from the stable regime where at least half of the population $|c_0|^2$ persists. For $\Delta_e = -\omega_r$, the critical pump photon number for entering the unstable regime is smallest since light scattered from the initial condensate is recoil shifted by one ω_r . For $\Delta_e < -\omega_r$, the phase boundary between the stable and the unstable regime follows the prediction of a numerical simulation, which ignores the pinning potential (solid line in the left and right subplots). Evidently, the pinning potential has only little effect in this regime. This is because at threshold, the system jumps from a homogeneous superfluid state directly into a state where the atoms form a density grating that moves with a finite start velocity [12]. In the reference frame of the moving atoms, the pinning potential averages out and has no effect. On the contrary, for positive detuning, the atoms form a stationary density grating which can be seeded efficiently by the pinning potential. In fact, the observed phase boundary steeply increases in this regime and asymptotically approaches a vertical line positioned at a critical detuning of $\Delta_0 \simeq 0.7\omega_r$ (dashed line in the left and right subplot). A numerical simulation which includes pinning, reproduces this behavior (right subplot).

The theoretical analysis of the experiment describes

the light in the pump mode and the probe mode by the field operators $\hat{A}_p = \hat{a}_p e^{ikz}$ and $\hat{A} = \hat{a} e^{-ikz}$. The atomic matter field $\hat{\psi} = \sum \hat{c}_n e^{2inkz}$ is expanded into momentum eigenstates, separated by $2\hbar k$, which is the momentum transferred to the atoms by scattering a single photon from the pump mode into the probe mode. The atoms and the light interact via the optical dipole potential $H_{\text{int}} = \hbar U_0 \int \hat{\psi}^\dagger \hat{\psi} (\hat{A}_p + \hat{A}) (\hat{A}_p^\dagger + \hat{A}^\dagger) dV$. Mirror scattering couples the pump mode with the probe mode and forms the pinning potential, $H_p = -\hbar \kappa_s (\hat{A}_p \hat{A} + \hat{A}_p^\dagger \hat{A}^\dagger)$. The equations of motion are derived from the Hamiltonian $H = H_0 + H_{\text{int}} + H_p$ with $H_0 = \int [\psi^\dagger (-\hbar^2 \nabla^2 / (2m)) \psi + \hbar \Delta_c (A^\dagger A + A_p^\dagger A_p)] dV$. Since the chemical potential of the condensate is much smaller than the recoil energy, the small contributions due to atom-atom interaction are neglected. In mean field approximation, operators are replaced by their expectation values a_p , a , and c_n . Since the power of the pump mode is electronically stabilized we set a_p to be constant. Because only the relative phase between a and a_p is physically relevant we also set $a_p = |a_p|$. For the equations of motion one then gets [9]

$$\dot{c}_n = -in^2 \omega_r c_n - i\sigma (c_{n-1} a^* + c_{n+1} a) \quad (1a)$$

$$\dot{a} = -(\kappa + i\Delta_e) a - i\sigma \sum_n c_n^* c_{n-1} - i\kappa_s |a_p| \quad (1b)$$

with the coupling constant $\sigma := U_0 |a_p|$ and the total number of atoms $N = \sum c_n^* c_n$. The finite cavity line width is taken into account by adding the decay term $-\kappa a$. The simulations in Fig. 2 are based on Eq. (1a, 1b) with the sum ranging from $n = -5$ to $n = 5$, since higher momentum states have not been observed for the chosen experimental parameters.

To gain further physical insight we interpret Eq. (1a, 1b) in the vicinity of the threshold. Higher momentum states with $|n| > 1$ can then be neglected yielding

$$\dot{c}_{-1} = -i\omega_r c_{-1} - i\sigma a c_0 \quad (2a)$$

$$\dot{c}_0 = -i\sigma (a c_1 + a^* c_{-1}) \quad (2b)$$

$$\dot{c}_1 = -i\omega_r c_1 - i\sigma a^* c_0 \quad (2c)$$

$$\dot{a} = -i\Delta a - i\sigma b - i\kappa_s |a_p|. \quad (2d)$$

Here, we introduce the complex detuning $\Delta = |\Delta| e^{i\delta} := \Delta_e - i\kappa$ and the complex structure factor $b = |b| e^{i\varphi_b} := c_1^* c_0 + c_0^* c_{-1}$. Without mirror scattering, the population of the zero momentum component $|c_0|^2$ remains undepleted until the system becomes unstable. In previous work, c_0 was thus approximated as constant near threshold. The equations then become linear and can be solved analytically [18, 19]. If mirror scattering is included, the resulting optical lattice potential depletes the zero momentum component even below threshold. Thus c_0 has to be kept variable and the equations resume their nonlinear character. Treating Eq. (2a-2d) by linearization

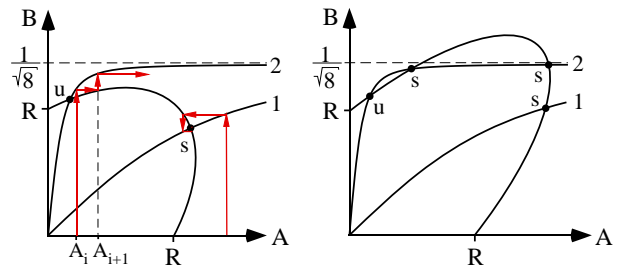


FIG. 3: Relation between the amplitudes of probe mode A and of structure factor B for weak and strong pumping (saturation curve 1 and 2) as well as small and large cavity pump detuning (left and right subplot). The stability of the equilibrium points at the intersection of the saturation curves with the ellipse (dots) can be determined geometrically (red arrows).

around the steady state solutions ($\dot{a} = \dot{c}_{0,\pm 1} = 0$) is not successful since a constant structure factor may exist, even if the coefficients $c_{\pm 1,0}$ are time dependent. The stability diagram can still be derived with the following strategy. In a first step, we solve the first three equations with $a = |a| e^{i\varphi_a}$ being regarded as a time independent parameter. The resulting linear eigenproblem can then be solved straight forward. It has three eigenstates, with one of them being a dark state that does not couple to the light field. The modulus of the structure factor for the two other states can be calculated to be

$$B = \frac{1}{\sqrt{8}} \frac{A/A_s}{\sqrt{1 + |A|^2/A_s^2}}. \quad (3)$$

Here, we introduce the normalized strength of the structure factor $B := |b|/(2N)$, the normalized amplitude of the light mode $A := |a||\Delta|/(2N\sigma)$ and the saturation parameter $A_s := |\Delta|\omega_r/(2\sqrt{8}N\sigma^2)$. For both states the structure factor is time independent and saturates at a maximum $B_m := 1/\sqrt{8}$ as A_s approaches zero for strong pumping. The two states differ in the limit of vanishing a , where the population $|c_0|^2$ approaches either zero or N . We thus ignore the first case since in the experiment all atoms are initially in the condensate. The calculation shows that for the second case the phases of the structure factor and the light field are equal, $\varphi_b = \varphi_a$. In a second step we determine how, vice versa, a given structure factor leads to a stable light field. Setting $\dot{a} = 0$ in Eq. (2d) yields

$$A^2 + B^2 + 2AB \cos \delta = R^2. \quad (4)$$

In Fig. 3, Eq. (3) and (4) are plotted. Eq. (4) forms an ellipse tilted by 45° . Its long axis varies between $2R$ (circle) for $\Delta_e = 0$ and infinity for $\Delta_e \gg \kappa$. Equilibrium states exist at the intersection points of both curves. The stability of equilibrium points are determined by reading from the diagram how a given field A_i results in a

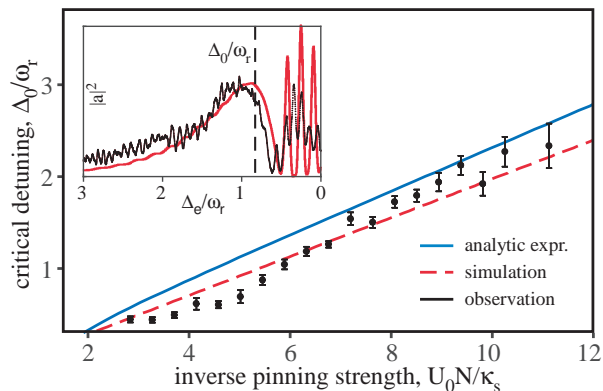


FIG. 4: Shift of the phase boundary Δ_0 with the inverse strength of the pinning potential. The observations (black dots), the simulations (red dashed line), and the analytic expression of Eq. (5) are in reasonable agreement. The inset shows the observed power in the probe mode during the quench (black line). We identify the phase boundary Δ_0 (dashed vertical line) as the position of the quick drop that follows the continuous increase while Δ_e approaches Δ_0 from above. The rapid oscillations for $\Delta_e < \Delta_0$ are typical for the unstable regime. The red line shows the result of a numerical simulation.

structure factor B (vertical arrows) and how the so determined B generates a new light field A_{i+1} (horizontal arrows). By repeating this sequence, the resulting series A_i converges for stable equilibrium and diverges otherwise. For small detuning (left subplot) and weak pumping (saturation curve 1) one finds a single point of stable equilibrium (indicated by "s"). For stronger pumping, the point moves to smaller A and eventually becomes unstable (saturation curve 2, "u"). Without condensate depletion (neglecting the second term in the square root of Eq. (3)) the system becomes unstable for $A_s = 1/\sqrt{8}$ which reproduces the threshold behavior found in previous models [12, 18, 19]. For large detuning, the stable point remains stable even for large pumping. This is true for arbitrary pump strength only if the maximum of the ellipse $R/\sin(\delta)$, exceeds the maximum value of the structure factor B_m (dashed line). This condition determines the critical detuning $\sin(\delta_0) = R/\sqrt{8}$. After replacing the above definitions, the critical detuning defining the vertical phase boundary in the limit of strong pumping reads

$$\frac{\Delta_0}{\kappa} = \sqrt{\frac{1}{8} \left(\frac{2U_0N}{\kappa_s} \right)^2 - 1}. \quad (5)$$

It depends on the strength of the pinning potential κ_s via the ratio $1/R = 2U_0N/\kappa_s$. Compared to this analytical expression, numerical analysis shows a shift of the threshold to smaller detunings for lower pumping strengths. We tested this relation by recording the phase boundary for various mirror scattering κ_s and atom number N . The phase boundary is detected by sweeping the detuning Δ_e

from large to small values within 1 ms, while the photon number in the pump mode is electronically stabilized to a constant value of $|a_p|^2 = 4 \times 10^6$ (inset in Fig. 4). While sweeping, the power in the probe mode increases until eventually the threshold is reached. We identify the critical detuning Δ_0 at the edge, where the power in the probe mode drops quickly and the system becomes unstable. By repeating the experiment for various values of NU_0/κ_s we obtain the curve in the main graph of Fig. 4. The observations (black dots), the simulation (red dashed line) and the analytic expression (Eq. (5), blue line) are in reasonable agreement. In the absence of a pinning potential, previous theoretical models [18] predict strict threshold behavior only for lossless cavities. If losses are included, the threshold smears out and the system becomes unstable even for infinitesimally low pump power. Our observations, however, support a physical picture (Fig. 3) that predicts strict threshold behavior also for lossy cavities and even in the limit of vanishing injection ($R \rightarrow 0$).

In summary, we have investigated an atomic Bose Einstein condensate in an optical ring resonator with additional pinning potential. A stable phase was identified above a critical cavity pump detuning. The phase boundary is defined by the competition of the pinning potential and the optical potential generated by the atoms. The observations are quantitatively described by simulating the nonlinear equations of motion, including depletion of the condensate. A geometric interpretation is introduced to determine equilibrium and stability of the system and an analytic expression for the phase boundary is derived in the limit of strong pumping. By seeding the probe mode, the transition from a ring geometry to a standing wave geometry can be explored similar as in recent work with a condensate replaced by a nano membrane [20]. More work is required to understand the role of the two additional points of equilibrium which appear above the critical detuning. Also unclear is the classification of the phase transition, quantum fluctuations near threshold and possible metastability [21].

We acknowledge helpful discussion with Andreas Hemmerich, Martin Schmidt and Peter Domokos. This work has been supported by the Deutsche Forschungsgemeinschaft (ZI 419/8-1) and by ColOpt – EU H2020 ITN 721465.

* simon.schuster@uni-tuebingen.de

† claus.zimmermann@uni-tuebingen.de

- [1] J. Klinder, H. Keßler, M. Wolke, L. Mathey, A. Hemmerich, *PNAS* **112**(11) 3290-3295 (2015); J. Klinder, H. Keßler, M. Reza Bakhtiari, M. Thorwart, and A. Hemmerich, *Phys. Rev. Lett.* **115**, 230403 (2015); M. Wolke, J. Klinder, H. Keßler, A. Hemmerich,

- Science* **337**, 75-78 (2012).
- [2] R. Landig, L. Hruby, N. Dogra, M. Landini, R. Mottl, T. Donner and T. Esslinger, *Nature* **532**, 476 (2016).
- [3] J. Léonard, A. Morales, P. Zupancic, T. Donner, and T. Esslinger, *Science* **358**, 1415-1418 (2017); J. Léonard, A. Morales, P. Zupancic, T. Esslinger, and T. Donner, *Nature* **543**, 87 (2017).
- [4] K. E. Ballantine, B. L. Lev, and J. Keeling, *Phys. Rev. Lett.* **118**, 045302 (2017); V. D. Vaidya, Y. Guo, R. M. Kroeze, K. E. Ballantine, A. J. Kollár, J. Keeling, and B. L. Lev, *Physical Review X* **8**, 011002 (2018).
- [5] J. Kohler, J. A. Gerber, E. Dowd, and D. M. Stamper-Kurn, *Phys. Rev. Lett.* **120**, 013601 (2018).
- [6] F. Mivehvar, S. Ostermann, F. Piazza, H. Ritsch, *Phys. Rev. Lett.* **120**, 123601 (2018).
- [7] B. Megyeri, G. Harvie, A. Lampis, and J. Goldwin *Phys. Rev. Lett.* **121**, 163603 (2018).
- [8] D. S. Naik, G. Kuyumjian, D. Pandey, P. Bouyer, A. Bertoldi *Quantum Sci. Technol.* **3** 045009 (2018).
- [9] N. Piovella, M. Gatelli, R. Bonifacio, *Opt. Commun.* **194**, 167 (2001).
- [10] D. Kruse, Ch. von Cube, C. Zimmermann, Ph.W. Courteille, *Phys. Rev. Lett.* **91**, 183601 (2003).
- [11] S. Slama, S. Bux, G. Krenz, C. Zimmermann, Ph.W. Courteille, *Phys. Rev. Lett.* **98**, 053603 (2007).
- [12] D. Schmidt, H. Tomczyk, S. Slama, and C. Zimmermann, *Phys. Rev. Lett.* **112**, 115302 (2014).
- [13] H. Tomczyk, D. Schmidt, C. Georges, S. Slama, and C. Zimmermann, *Phys. Rev. A* **91**, 063837 (2015).
- [14] C. Emary and T. Brandes, *Phys. Rev. E* **67**, 066203 (2003).
- [15] K. Baumann, C. Guerlin, F. Brennecke, and T. Esslinger, *Nature* **464**, 1301 (2010); K. Baumann, R. Mottl, F. Brennecke, and T. Esslinger, *Phys. Rev. Lett.* **107**, 140402 (2011); R. Mottl, F. Brennecke, K. Baumann, R. Landig, T. Donner, and T. Esslinger, *Science* **336**, 1570-1573 (2012);
- [16] S. Bux, G. Krenz, S. Slama, C. Zimmermann, Ph.W. Courteille, *Appl. Phys. B* **89**(2-3), 181-186 (2007).
- [17] G. Krenz, S. Bux, S. Slama, C. Zimmermann, Ph.W. Courteille, *Appl. Phys. B* **87**(4), 643-647 (2007).
- [18] M. G. Moore, O. Zobay, and P. Meystre, *Phys. Rev. A* **60**, 1491 (1999).
- [19] F. Dimer, B. Estienne, A. S. Parkins, and H. J. Carmichael, *Phys. Rev. A* **75**, 013804 (2007).
- [20] A. Yilmaz, S. Schuster, P. Wolf, D. Schmidt, M. Eisele, C. Zimmermann and S. Slama, *New J. Phys.* **19**, 013038 (2017).
- [21] L. Hruby, N. Dogra, M. Landini, T. Donner, and T. Esslinger, *PNAS* **115**(13) 3279-3284 (2018).